J Appl Electrochem (2008) 38:1097–1110
DOI 10.1007/s10800-008-9562-y

ORIGINAL PAPER

Temperature programmed desorption of oxygen from Pd films interfaced with Y_2O_3-doped ZrO_2

A. Katsaounis

Received: 21 February 2008 / Revised: 26 March 2008 / Accepted: 4 April 2008 / Published online: 29 April 2008

Abstract The origin of the effect of non-faradaic electrochemical modification of catalytic activity (NEMCA) or Electrochemical Promotion was investigated via temperature-programmed-desorption (TPD) of oxygen, from polycrystalline Pd films deposited on 8 mol%Y_2O_3–stabilized–ZrO_2 (YSZ), an O^{2-} conductor, under high-vacuum conditions and temperatures between 50 and 250 °C. Oxygen was adsorbed both via the gas phase and electrochemically, as O^{2-}, via electrical current application between the Pd catalyst film and a Au counter electrode. Gaseous oxygen adsorption gives two adsorbed atomic oxygen species desorbing at about 300 °C (state β_1) and 340–500 °C (state β_2). The creation of the low temperature peak is favored at high exposure times (exposure >1 kL) and low adsorption temperatures ($T_{ads} < 200$ °C). The decrease of the open circuit potential (or catalyst work function) during the adsorption at high exposure times, indicates the formation of subsurface oxygen species which desorbs at higher temperatures (above 450 °C). The desorption peak of this subsurface oxygen is not clear due to the wide peaks of the TPD spectra. The TPD spectra after electrochemical O^{2-} pumping to the Pd catalyst film show two peaks (at 350 and 430 °C) corresponding to spillover O_{ads} and $O^{\delta-}_{ads}$ according to the reaction:

$$O^{2-}_{(YSZ)} \rightarrow O^{\delta-}_{ads} \rightarrow O_{ads}$$

The formation of the spillover $O^{\delta-}_{ads}$ oxygen species is an intermediate stage before the formation of the atomic adsorbed oxygen, O_{ads}. Mixed gaseous and electrochemical adsorption was carried out in order to simulate the Electrochemical Promotion conditions. The initial surface coverage with oxygen from the gas phase plays a very important role on the high or low effect of polarization. In general mixed adsorption leads to much higher oxygen coverages compare with that observed either under gaseous or electrochemical adsorption. The binding strength of the atomic adsorbed oxygen (state β_2) was investigated as a function of applied potential. It was found that the binding energy decreases linearly with increasing catalyst potential and work function. Similar behavior has been observed for oxygen adsorption on Pt, Ag and Au deposited on YSZ in previous studies.

Keywords Temperature programmed desorption · Oxygen adsorption on Pd · Electrochemical promotion · Electrochemical adsorption · Palladium supported catalyst · Spillover-backspillover of oxygen · NEMCA effect

A. Katsaounis (✉)
Department of Environmental Engineering, Technical University of Crete, 73100 Chania, Greece
e-mail: alex.katsaounis@enveng.tuc.gr

1 Introduction

1.1 Oxygen adsorption on Pd surfaces

The interaction of oxygen with palladium catalysts and single crystals has been the subject of many fundamental studies. The interest for this system arises mainly from the importance of palladium as a catalyst for oxidizing hydrocarbons or CO. Also Pd consists a promising catalyst for applications involving other oxidation reactions including automotive catalytic converters and catalytic combustion of methane in advanced gas turbines where ultralow NO_x emission are desired. Therefore, numerous surface science techniques have been used to study the adsorption of O_2 on Pd along with theoretical studies [1–21]. The studies have been carried out on single crystals [1–21], polycrystalline samples [19], supported catalyst [20, 21] in the temperature

range between −173 and 500 °C from UHV to atmospheric pressure conditions. The first studies concerning oxygen adsorption on palladium, date back to the late 1960s by Ertl et al. [1, 2] using LEED and mass spectrometer techniques. In 1969 Ertl and Rau [1] were the first who studied the oxygen adsorption on Pd (110) and the catalytic reaction of CO and O_2 over Pd (110).

Numerous studies have been reported concerning oxygen adsorption on single crystals. Conrad et al. [3, 4] observed wide oxygen peaks during oxygen desorption while they have established that oxygen tends to penetrate the Pd (111) surface at high temperatures. For adsorption temperatures above 427 °C bulk diffusion took place. The existence of a broad peak of atomic oxygen (T_p = 500–550 °C) have been reported also by Matsushima [5] for the case of oxygen adsorption on Pd (111) at −173 °C. He also observed repulsive interactions between the oxygen species as the oxygen coverage was increased. The repulsive interactions between the surface oxygen species have been also reported by Guo et al. [6] using Pd (111) at adsorption temperature −173 °C. Weissman et al. [7] refers to the existence of two states of oxygen, on Pd (111), at room temperature, one on the surface (T_p = 560 °C) and one beneath it (T_p = 870 °C). Giving an answer to where oxygen can be adsorbed Imbihl et al. [8] using EELS and LEED technique suggest that at room temperature, atomic oxygen adsorbs on the three fold sites of Pd (111) giving a peak in the EELS spectrum at 480 cm^{-1}. This peak is characteristic of the perpendicular vibration of oxygen atoms adsorbed in the threefold adsorption sites. In order to study the oxidation of Pd (111) and the surface reconstruction Zheng et al. [9] used STM, TPD and LEED. Initial exposure of Pd (111) to oxygen gave a single TPD peak at 577 °C at low coverage and at 527 °C as the coverage was increased indicating repulsive interactions. As the coverage was increased more, a peak at 452 °C developed and gradually began to replace the 527 °C peak. Using LEED, AES and XPS, Voogt et al. [10] reported that at elevated temperatures (T > 197 °C) and pressures above 10^{-4} Pa three stages in the interaction of oxygen with Pd (111) could be distinguished, (a) surface oxygen, (b) diffusion of oxygen into the surface layer(s) and (c) nucleation and formation of a surface oxide. No diffusion to the bulk or even to the subsurface layers was observed under any condition studied by Voogt et al.

Many studies also have been published regarding oxygen adsorption on other single crystals as Pd (100) and Pd (110) [11–19]. Stuve et al. [11], on Pd (100), at room temperature reported three temperature programmed desorption states at 567 °C, 457 °C and 422 °C while repulsive interactions have been observed between the oxygen species of state α (567 °C). The data of Chang et al. [12] concerning thermal desorption studies of oxygen on Pd (100) show that at adsorption temperature −73 °C there is a single desorption peak of atomic oxygen (T_p = 450–540 °C) with a maximum which shifts to lower temperatures as the coverage increases indicating repulsive interactions. In addition oxygen TPD at 27 and 123 °C show the existence of two other peaks of oxygen at lower temperatures due to the surface reconstruction. The same result reported by Klier et al. [13] who observed the reconstructions on Pd (100) from p(2 × 2) to c(2 × 2) to p(5 × 5) and finally to $(\sqrt{5}x\sqrt{5})$R27°. Thermal desorption of oxygen from Pd (110) for adsorption temperatures above room temperature have been reported by He et al. [14, 15]. According to their results for adsorption temperature 202 °C two oxygen peaks observed during the desorption, one at 540 °C at lower exposure associated with atomic oxygen and another one at higher exposure at 450 °C. He et al. suggested that the decrease of the work function with increasing oxygen exposure during the adsorption is associated with this low temperature oxygen. For this reason they conclude that this weakly bonded oxygen maybe associated with the formation of an oxide or the incorporation of oxygen atoms below the plane of the surface, hence inverting the sign of the dipole layer compared to adsorption above the plane. The population of the weakly bonded oxygen, according to He et al. [15] is much slower at elevated temperature. For adsorption temperature 303 °C, one single oxygen peak was observed. Bondzie et al. [16] also, using XPS and UPS have shown that adsorbed oxygen at room temperature exists on Pd (110) in two states, a surface (T_p = 545 °C) and a more weakly bound state (T_p = 460 °C) designated as ''subsurface'' oxygen and associated with the work function decrease during the adsorption period. The data of Milun et al. [17], on Pd (110), for adsorption temperatures above 327 °C showed two thermal desorption peaks at 427 and 497 °C. The existence of the second weekly bonded oxygen on Pd (110) at 200 °C was confirmed also by Yagi et al. [18]. Studying a polycrystalline Pd film Campbell et al. [19] observed that oxygen penetrates into the bulk of Pd, for adsorption temperatures above 250 °C.

In addition to the studies concerning oxygen adsorption on single crystals a few studies have been carried out involving oxygen adsorption on supported catalysts. Oxygen desorption from Pd supported on a-Al_2O_3 (0001) catalyst carried out by Putna et al. [20]. They have shown that on large Pd particles there are two unresolved peaks near 527 and 602 °C while the results for smaller Pd particles exhibit desorption in a much narrower temperature window, from 577 to 727 °C, with a peak maximum near 677 °C. Oxygen TPD studies from model catalysts prepared by evaporating palladium on a silica thin film supported on a Mo(110) substrate reported by Xu et al. [21]. They observed for adsorption temperature 27 °C one

single peak (T_p = 527–577 °C) with repulsive interactions between the oxygen species.

The main conclusions that could be drawn from the above studies are the following:

(i) On single crystals Pd (111) [1–10] oxygen desorbs in a single wide peak between 500 and 580 °C. Repulsive interactions are grown between the oxygen adsorbed species.

(ii) On single crystals Pd (110) and Pd (100) [11–18], a second peak observed between 420 and 480 °C. The population of this weakly bonded oxygen is much slower at elevated temperatures while repulsive interactions have been reported between the high temperature oxygen species.

(iii) Oxygen tends to penetrate the Pd surface at high temperatures and exposures. There is still a confusion concerning what we call ''subsurface'' oxygen for the case of Pd. In a few studies [14–16] the decrease of the work function during the adsorption at high exposure times is associated with a ''subsurface'' weakly bonded oxygen. This is not in agreement with the ''subsurface oxygen theory'', which considers that this kind of oxygen is strongly bonded oxygen and desorbs at higher temperatures than surface oxygen. Besides, the existence of the subsurface oxygen as a strongly bonded oxygen on Pd (111) (T_p = 870 °C) was reported by Weissman [7] and other authors. The penetration of oxygen into the bulk can happen even in the case of polycrystalline Pd [19].

(iv) Oxygen adsorption on supported catalysts [20, 21] have been carried out and show, during desorption, one single wide oxygen peak or two very close peaks that shift to lower temperatures indicating repulsive interactions.

(v) Surface reconstruction is taking place with coverage increase having as a result the presence of new peaks in the oxygen TPD spectra.

1.2 Electrochemical promotion of catalysis (EPOC)

It has been found that the catalytic activity and selectivity of metals interfaced with solid electrolytes can be altered dramatically and reversibly by application of an electrical current or potential between the metal catalyst film and a second metal film (counter-electrode) also deposited on the solid electrolyte [22–28]. The increase in catalytic rate can be several, typically two to five, orders of magnitude higher than that anticipated from Faraday's Law [22–28]. Considering as example polycrystalline Pd catalyst films deposited on Y_2O_3–stabilized–ZrO_2 (YSZ), exposed to methane-oxygen mixtures, electrochemical O^{2-} supply causes a catalytic oxidation rate increase, Δr, which is typically 10^2 times higher than the rate, I/2F, of O^{2-} supply to the catalyst [29, 30]. Therefore, each O^{2-} supplied to the catalyst causes 10^2 chemisorbed oxygen atoms to react with methane and form CO_2. This phenomenon of Electrochemical Promotion, also known in the literature as non-faradaic electrochemical modification of catalytic activity (NEMCA effect), is of considerable theoretical and potentially practical importance.

During the last twenty years, the NEMCA effect has been studied for over sixty different catalytic systems on Pt, Rh, Pd, Ag, Ni, Au, IrO_2 and RuO_2 catalyst films deposited on O^{2-}, F^-, Na^+ and H^+ conducting solid electrolytes [25–40] as well as mixed electronic-ionic conductors, such as TiO_2 [41], and aqueous alkaline solutions [42] using both lab scale reactors [25–41] and novel monolithic reactors [43, 44]. The importance of NEMCA in catalysis [45], surface science [46] and electrochemistry [47] has been discussed and work prior to 2001 has been reviewed [22, 23, 27, 28]. Despite the large number of different ionic conductors which have been used to induce and study electrochemical promotion most of the work in this area has utilized YSZ as solid electrolyte.

Palladium polycrystalline films supported on YSZ have been used in NEMCA studies to enhance the rate of C_2H_4 oxidation [29–48], CH_4 oxidation [29, 30] and NO reduction by CO [49, 50], in the temperature range between 290 and 477 °C.

The enhancement factor or Faradaic efficiency, Λ, is defined as:

$$\Lambda = \Delta r/(I/2F) \quad (1)$$

where Δr is the electrochemically induced change in catalytic rate (expressed in mol O/s), I is the applied current (defined positive when anions are supplied to the catalyst) and F is Faraday's constant. Λ values range from -700 to 10^4 for the case of palladium films [27, 28]. Both electrophobic ($\Lambda > 1$) and electrophilic ($\Lambda < -1$) behavior has been noticed.

The rate enhancement ratio, ρ, is defined as:

$$\rho = r/r_o \quad (2)$$

where r is the electrochemically promoted catalytic rate and r_o is the open-circuit (unpromoted) catalytic rate value, reaches a maximum value of 90 for CH_4 oxidation [30], but is typically between 1.45 and 4.2 for ethylene oxidation [48] and NO reduction by CO [49].

The origin of electrochemical promotion has been investigated using a variety of techniques including STM [51–53], XPS [54], SERS [32–55], TPD [56–61], UPS [62] and the Kelvin probe method [26, 63, 64]. A key step in the elucidation of the origin of NEMCA was the experimental discovery [26, 27, 62] and theoretical confirmation [25]

that solid electrolyte cells with metal electrodes are both work function probes and work function controllers for the gas-exposed surfaces of their electrodes. Both Kelvin probe [26, 63, 64] and UPS [62] measurements have shown that:

$$eU^{o}_{WR} = \Phi_W - \Phi_R \quad (3)$$

$$e\Delta U_{WR} = \Delta(\Phi_W) \quad (4)$$

where U_{WR} is the catalyst-working electrode potential, U^{o}_{WR} stands for the open-circuit potential and Φ_W and Φ_R are the average work functions of the working and reference electrodes, respectively. Equations (3) and (4) are also consistent with the spillover/backspillover ion mechanism proposed to explain the effect of the electrochemical promotion. The change in the work function upon application of an external potential ΔU_{WR} is due to the migration of ionic species on the gas-exposed catalyst-electrode surface.

Considering the example of Pd supported on O^{2-} conducting solid electrolytes, like YSZ, positive current application means oxygen ions pumping through the solid electrolyte to the palladium catalyst-working electrode. These ions can follow two possible pathways. Oxygen ions can dispose of their charge at the three-phase boundaries and form spillover dipoles which can spread over the catalyst surface. In addition to this charge transfer (electrocatalytic) mechanism, there is another possibility due to the finite solubility of oxygen in Pd; oxygen ions go through the Pd as dissolved oxygen and then emerge at the catalyst surface giving rise to the formation of covalently bonded chemisorbed oxygen. Both oxygen species cause an increase on catalyst work function.

In previous studies [56–61], detailed TPD experiments were reported utilizing Pt and Ag films interfaced with YSZ providing a direct explanation for electrochemical promotion effect in Pt/YSZ and Ag/YSZ systems. In this study using the same technique of TPD, we present the results of oxygen adsorption on Pd deposited on YSZ and analyze the effect of applied potential on the binding strength of adsorbed oxygen.

2 Experimental

2.1 Catalyst preparation and characterization

The gold reference and counter electrodes were deposited on one side of the YSZ disk (Dynamic-Ceramic; diameter 19 mm; thickness 2 mm) by application of a thin coating of an Engelhard A-1118 paste and calcining in air at 400 °C for 2 h and then at 850 °C for 30 min. The catalyst (working electrode) consisted of a thin Pd film deposited on the other side of the YSZ disk using a thin coating of an Engelhard A-2985 paste calcined in air at 450 °C for 6 h. The sample was then placed in a quartz tube and PdO reduced in a flow of 60 ml/min of 1% H_2 in He, at 60 °C for 30 min and then it was heated up to 300 °C with the same H_2 flow rate. A three-electrode cell arrangement was constructed according to the previous procedure. The superficial surface area of the Pd film was 2.8 cm^2 and its true surface area was 475 cm^2 (considering an average surface density for polycrystalline Pd of 1.27×10^{19} atoms/m^2 [65]). The active surface area was computed by the isothermal titration technique [28, 66], i.e. by measuring the reactive oxygen uptake via carbon monoxide titration with O_2 at atmospheric pressure and temperatures between 300 and 400 °C as described in detail elsewhere [28]. The maximum reactive oxygen uptake N_o (1.6×10^{-7} mol of O) was extracted under atmospheric conditions after the TPD experiments. The initial exposure of the sample to high temperatures during the heating (800 °C for a few seconds) probably results to a small decrease of the active surface area (N_o) compared with that after the preparation of the sample. However, since the highest temperature during the desorption was always the same, the extracted values of oxygen coverage (resulting from the total adsorbed oxygen and the N_o) can be assumed to be quite reliable. For the TPD measurements only one Pd/YSZ/Au cell was used. Gaseous, electrochemical and mixed adsorption were carried out using the same sample.

The catalyst was cleaned in the vacuum system. The "clean-up" procedure includes the treatment of surface with oxygen from the gas phase or with electrochemically supplied oxygen from the solid electrolyte followed by temperature programmed desorption. This resulted in a gradual increase of the amount of oxygen desorbing after a fixed dose. At the end of the "clean-up" treatment a reproducible oxygen desorption spectrum was achieved. Furthermore, no CO signal was detected during TPD, which is a good indication for the absence of carbon on the surface.

A series of blank TPD experiments showed that the YSZ specimen and the Au electrodes did not desorb any measurable amount of oxygen. Thus all the TPD spectra reported here can safely be attributed to oxygen chemisorption from the Pd film only.

2.2 Experimental apparatus

For all the experiments the disk was placed in an ultra high vacuum chamber, with a base pressure after baking of about 10^{-9} Torr (Fig. 1). The vacuum chamber was equipped with a quadruple mass spectrometer (Balzers QMG 420) and a leak valve gas inlet system. The signal of the spectrometer was calibrated to give the desorption rate, dN/dt, in mol O/s.

The sample was heated radiatively using an Osram xenon lamp located above the catalyst film (Fig. 1).

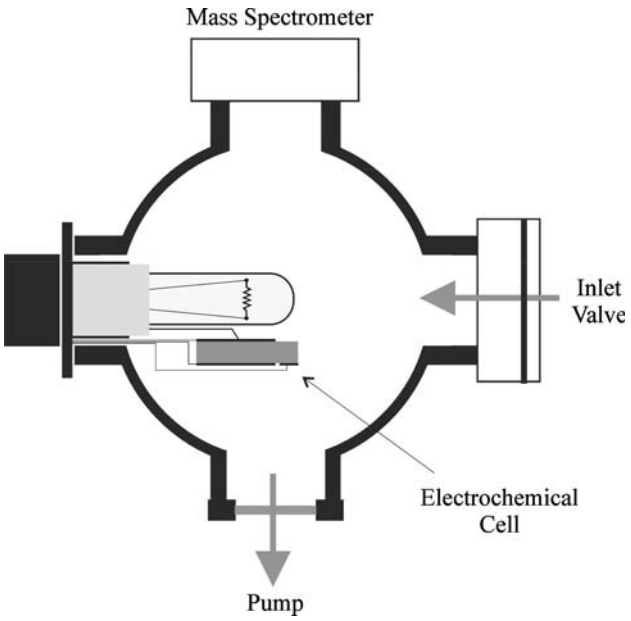

Fig. 1 Schematic of the vacuum chamber equipped with a mass spectrometer (BALZERS QMG 420) and a leak valve gas inlet system. The electrochemical cell shown inside consists of the solid electrolyte (YSZ), the Pd film catalyst-working electrode (WE) and, the Au counter (CE) and reference (RE) electrodes

A type-K thermocouple, attached on the Pd surface was used to measure the temperature. The temperature was varied linearly using a Eurotherm programmable temperature controller with a maximum heating rate of 2 °C/s.

Constant currents between the Pd film and the Au counter electrode (galvanostatic operation) were applied by an AMEL 2053 galvanostat–potentiostat. Furthermore, using the above type of galvanostat–potentiostat it was possible to monitor continuously the potential, U_{WR}, of the Pd film with respect to the Au-reference electrode under open circuit conditions.

Using equation (4), which relates the change in catalyst potential, U_{WR}, with the induced change in catalyst work function Φ, it was possible to monitor the change of the average work function of the polycrystalline Pd film during the adsorption and desorption experiments.

2.3 Oxygen adsorption

For the oxygen adsorption on the Pd film three different experimental procedures were used between 50 and 250 °C as follows:

1. *Gaseous adsorption.* The Pd/YSZ film was exposed to an oxygen pressure, P_{O_2}, of the order of 10^{-5} Torr for various exposure times, t_{O_2}, corresponding to several kilolangmuirs (1 kL = 10^{-3} Torr·s). The O_2-gas was injected to the vacuum chamber through a leak-valve.
2. *Electrochemical adsorption.* Oxygen was supplied to the Pd/YSZ film at a rate I/2F using a positive current, I, applied between the Pd film and the Au-counter electrode for various times. In this case the oxygen is locally depleted from the YSZ solid electrolyte in the vicinity of the Au-counter electrode without any loss in cell reversibility.
3. *Mixed adsorption.* This experiment consisted of a mixed gas and electrochemical adsorption. In this case the film was first exposed to an oxygen pressure, $P_{O_2} = 10^{-5}$ Torr for a certain time, t_{O_2}, followed by electrochemical supply of oxygen through the solid electrolyte for a time t_I.

In all the above experimental setups the adsorption temperature was varied between 50 and 250 °C. After oxygen adsorption, the sample was cooled rapidly under open circuit, followed by a linear increase of temperature with a heating rate β (°C/s) in order to obtain the TPD spectra.

For the determination of oxygen desorption activation energy, E_d, and its dependence on catalyst potential a series of low coverage TPD experiments were performed. The exact experimental procedure followed in this case was presented in detail in previous studies [56, 57]. The data were analyzed using both the standard Redhead analysis, as generalized by Falconer and Madix [67], as well as the low coverage method analysis using the initial slopes of the TPD spectra [68, 69].

3 Results and discussion

3.1 Gas phase adsorption

Figure 2a, b shows the oxygen thermal desorption spectra after the exposure of the Pd film to oxygen for various times. The exposure times, expressed in kL, are shown in the two figures. For high adsorption temperature (250 °C) one single wide peak is obtained (state β_2), attributed to the dissociatively chemisorbed oxygen species. It should be noted that in the temperature range of the present study only atomic species can exist on the surface, since the molecular species on Pd are adsorbed at adsorption temperatures below −140 °C [5–8, 11, 14, 15, 70]. For low adsorption temperatures (50 °C) a second peak develops (state β_1), at lower desorption temperatures (T_p = 290–300 °C), as we increase the coverage. Between the oxygen species of β_2 state there are strong repulsive interactions, as one can infer from Fig. 2a where the peak desorption temperature of state β_2 shifts from 500 to 430 °C as the coverage increases. On the other hand almost no shift was observed on the peak temperature of the β_1 state. At higher adsorption temperature (250 °C) strong apparent repulsive interactions appear between the oxygen species of state β_2. Thus the TPD spectra show wide peaks without any

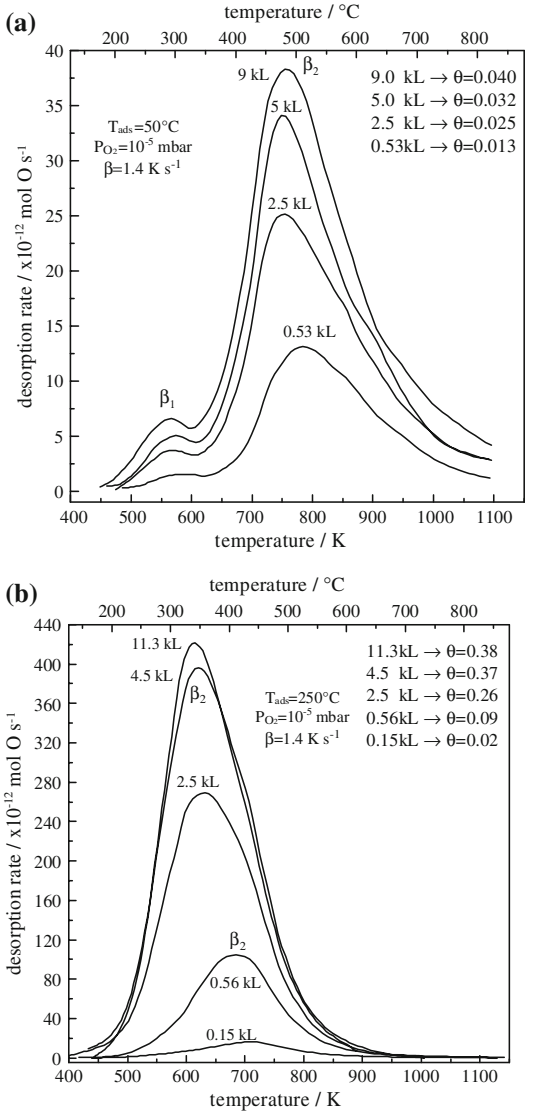

Fig. 2 Oxygen thermal desorption spectra after gaseous oxygen dosing for various exposure times at (**a**) 50 °C, $P_{O_2} = 1 \times 10^{-5}$ Torr and (**b**) 250 °C, $P_{O_2} = 1 \times 10^{-5}$ Torr. Oxygen exposure is expressed in kilolangmuirs (1 kL = 10^{-3} Torr·s). Desorption was performed with linear heating rate, $\beta = 1.4$ °C/s

separation between states β_1 and β_2. At 250 °C there is a shift of the desorption peak temperature from 450 to 340 °C. The above peak temperature values at high adsorption temperatures are in qualitative agreement with the reported values, 450–580 °C for Pd (111) single crystals [1–10].

In Fig. 3, in the temperature range 50–250 °C, the total amount of adsorbed oxygen increases as the adsorption temperature increases. It is clear that due to the repulsive interactions at high temperatures the two oxygen peaks overlap. The population of the weakly bonded oxygen, according to the data shown in Fig. 2a and b, is much lower at elevated temperatures.

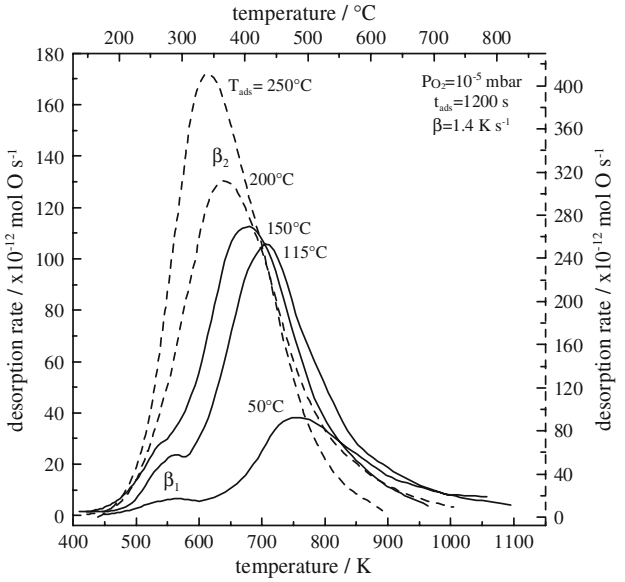

Fig. 3 Effect of the adsorption temperature on the total amount of adsorbed oxygen for five temperatures 50, 115, 200 and 250 °C. Desorption was performed with linear heating rate, $\beta = 1.4$ °C/s

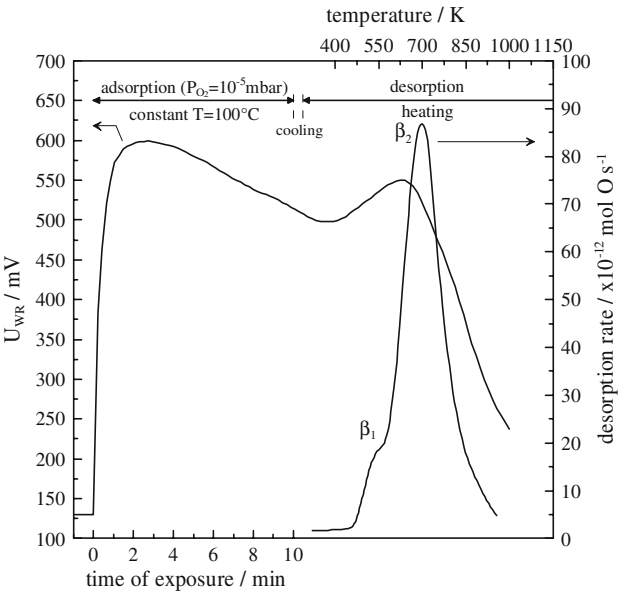

Fig. 4 Open circuit potential profile during adsorption and desorption for adsorption temperature T_{ads} = 100 °C. Desorption was performed with linear heating rate, $\beta = 1.4$ °C/s

In the case of adsorption at 100 °C the profile of the open circuit potential during adsorption and desorption is shown in Fig. 4. As expected, there is an initial increase of potential during oxygen adsorption due to the electron acceptor nature of adsorbed oxygen species. However, as the exposure time (exposure >1.5 kL) increases, we observe a decrease of the open circuit potential. Similar behavior was observed for all adsorption temperatures in

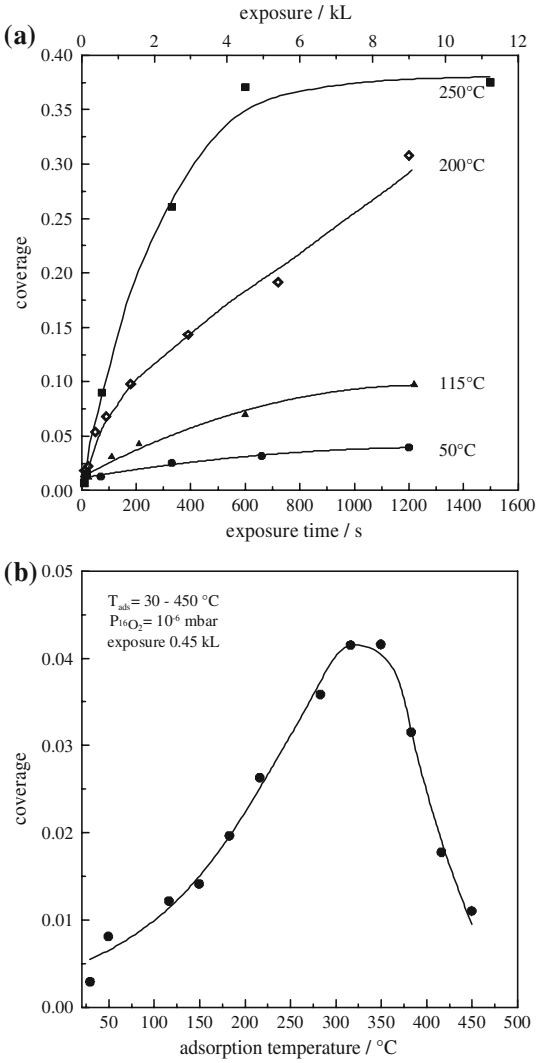

Fig. 5 (**a**) Adsorption profiles for oxygen adsorption at 50, 115, 200 and 250 °C. (**b**) Effect of adsorption temperature on oxygen coverage after constant exposure of 0.45 kL

the range of 50–250 °C. The potential decrease can be attributed to the formation of subsurface oxygen. On the other hand, the migration of the subsurface oxygen from the bulk to the surface can explain the initial increase of the work function during the desorption. This increase can also be explained assuming that during the desorption and depletion of the oxygen species the repulsive interactions are less and therefore the restored dipole moment is higher. The wide peaks shown in Fig. 2b, can be attributed to the poor separation of the subsurface oxygen. The ability of oxygen to penetrate Pd has been well known since 1977 [3, 4, 7, 19].

The oxygen adsorption profiles are shown in Fig. 5a for different adsorption temperatures. The oxygen coverages are computed from the corresponding TPD spectra using integration and the maximum reactive oxygen uptake $N_o = 1.6 \times 10^{-7}$ mol O measured via titration of adsorbed

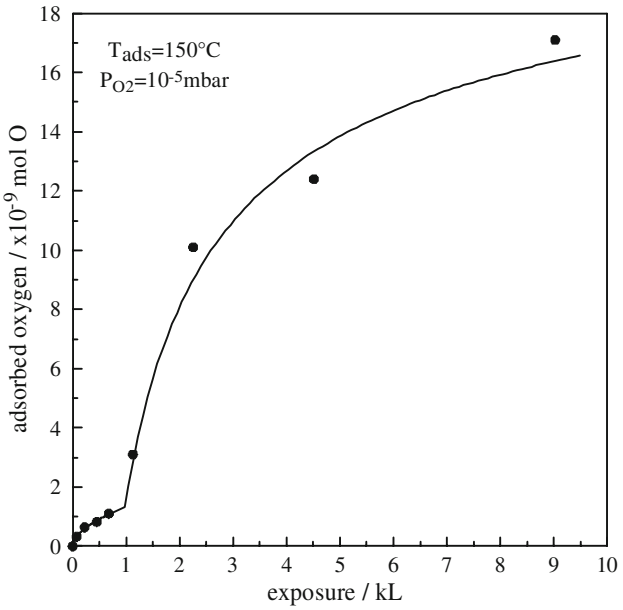

Fig. 6 Adsorption profiles for oxygen adsorption at 150 °C taking more data for exposures <1 kL

oxygen with CO at atmospheric pressure [28, 66]. The oxygen coverage increases as the adsorption temperature increases (range 50–250 °C). For higher temperatures ($T_{ads} > 300$ °C) the total oxygen coverage on the surface is much lower , as expected , due to oxygen desorption as observed in Fig. 5b.

For TPD experiments with oxygen exposures less that 1 kL the total amount of adsorbed oxygen tends to a constant value (Fig. 6 for the case of T_{ads} = 150 °C). However, for higher exposures there is a significant increase of oxygen coverage indicating some type of surface activation. Similar results are observed for all the adsorption temperatures. It is worth noting that similar previous studies with Pt/YSZ samples [60, 61] have shown that part of the total desorbed oxygen belongs to non-stoichiometric lattice oxygen ($^{16}O^{2-}$), coming from the solid electrolyte. Non-stoichiometric oxygen from the solid electrolyte (YSZ) can interact with oxygen from the gas phase (during gaseous adsorption) and finally be desorbed during the heating processes [60, 61].

The integral sticking coefficient for gas phase adsorption, S_g, is defined as the ratio of the adsorbed oxygen molecules (estimated from integration of the thermal desorption spectra) over the total oxygen molecules that collide with the surface, i.e., $(P_{O_2}/2\pi MRT_g)^{1/2} \cdot A \cdot t_{O_2}$, where P_{O_2} is the oxygen partial pressure in Nt/m^2, M is the molecular weight of O_2, R is the gas constant, T_g is the gas temperature in K, A is the total surface of the catalyst film and t_{O_2} is the oxygen exposure time. For gas phase adsorption the integral sticking coefficient is plotted against oxygen coverage in Fig. 7. The sticking coefficient varies between 6×10^{-5} and 6×10^{-3} and is strongly

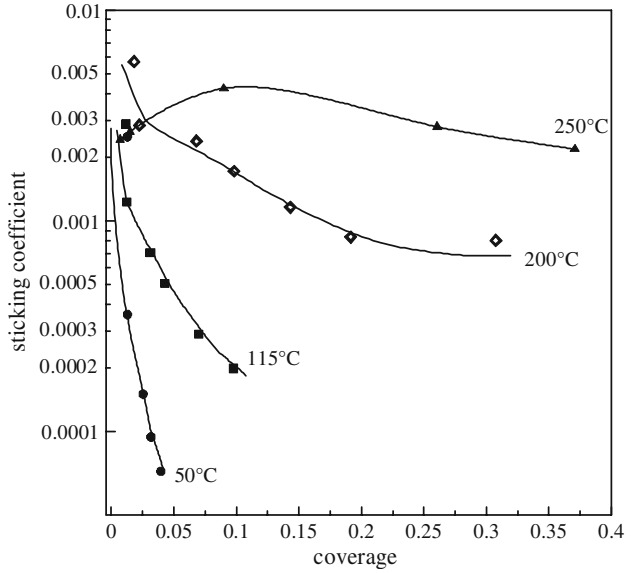

Fig. 7 Integrated sticking coefficient as a function of oxygen coverage during adsorption at 50, 115, 200 and 250 °C

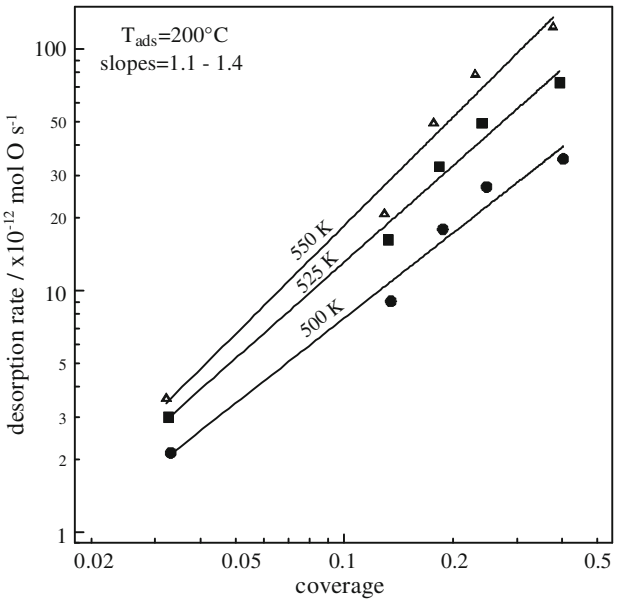

Fig. 8 Desorption rate isotherms obtained from the TPD spectra at T_{ads} = 200 °C indicating near- first order desorption

dependent on coverage and adsorption temperature. As expected, the coefficient, S_g, decreases with increasing coverage, with the exception at 250 °C where it appears to be practically constant. In all cases, the value of S_g is in the order of magnitude of the values reported for single crystal Pd (111) [5, 6, 18, 71–73].

Usually, the decrease in peak temperature with the increase in coverage is mostly due to second order desorption kinetics and less to repulsive interactions between the adsorbed species. Using the desorption spectra data, the above statement can be clarified by extracting the desorption order of β_2 state and thus the extent of the repulsive interactions. The basic desorption rate equation is expressed as:

$$\frac{dN}{dT} = (v/\beta) \cdot \theta^{v} \exp\left(-\frac{E_d}{RT}\right) \quad (5)$$

where v is the preexponential factor, n is the desorption order, and θ_o is the initial coverage.

By taking the logarithm of Eq. 5 we obtain:

$$\log(dN/dt) = \log v + n\log \theta - E_d/RT \quad (6)$$

The plot of ln(dN/dt) versus lnθ for constant temperature, is a straight line with a slope equal to n, if the desorption activation energy is weakly dependent on coverage. If we apply the above procedure at 200 °C we observe lines with a slope between 1.1 and 1.4; i.e., close to a first-order desorption (Fig. 8). Similar results were obtained for higher adsorption temperatures.

Comparing the results of previous studies concerning oxygen adsorption on Pd (111) [1–10] the polycrystalline Pd film surface mostly appears to consist of the (111) plane. It is worth noting that, although the coverages are quite small, one observes a pronounced decrease of the sticking coefficient when the oxygen coverage increases.

3.2 Electrochemical adsorption

Figures 9 and 10 show the oxygen thermal desorption spectra obtained after electrochemical O^{2-} supply to the Pd film through the solid electrolyte for two different temperatures, various currents, I, and different current application times, t_I. Contrary to the case of gas phase adsorption, one observes at high adsorption temperatures and high currents a shift of the peak desorption temperature to higher temperatures as the current application time or, equivalently, as the oxygen coverage increases (250 °C and 10 μA, Fig. 9a). These strong apparent attractive interactions between the adsorbed oxygen species are very clear at high adsorption temperatures. As shown below, these interactions are weaker at low temperatures and short current application times.

It is worth noting in Fig. 9b that the open circuit potential exhibits a constant value (plateau) at intermediate temperatures. An assumption of transformation between two phases can be made in order to explain the above behavior during the heating. It is noted that at high coverages (e.g. current application for long time) the value of the constant potential is always the same (U_{WR} = 625 mV for the case of 250 °C, Fig. 9b). Similar behavior was observed for all the adsorption temperatures. In order to investigate the existence of the two phases on the surface at low coverages, we performed TPD experiments at lower

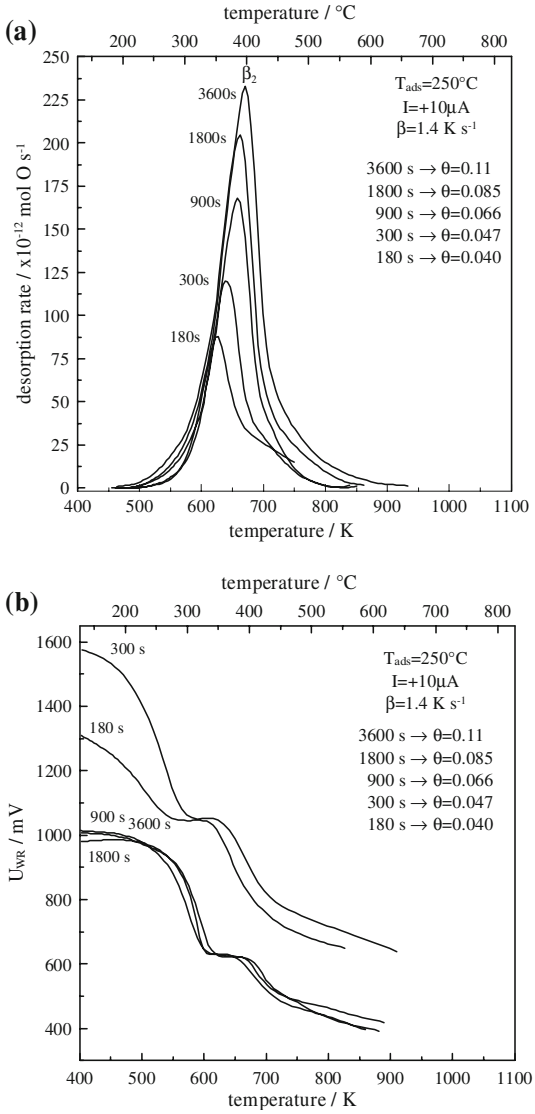

Fig. 9 (**a**) Oxygen thermal desorption spectra after electrochemical O^{2-} supply on the Pd film (I = +10 μA) through the solid electrolyte at 250 °C. The different curves correspond to various times of current application. Desorption was performed with linear heating rate, $\beta = 1.4$ °C s^{-1}. (**b**) Variation of Pd film potential versus Au reference electrode corresponding to the TPD spectra of Fig. 9a

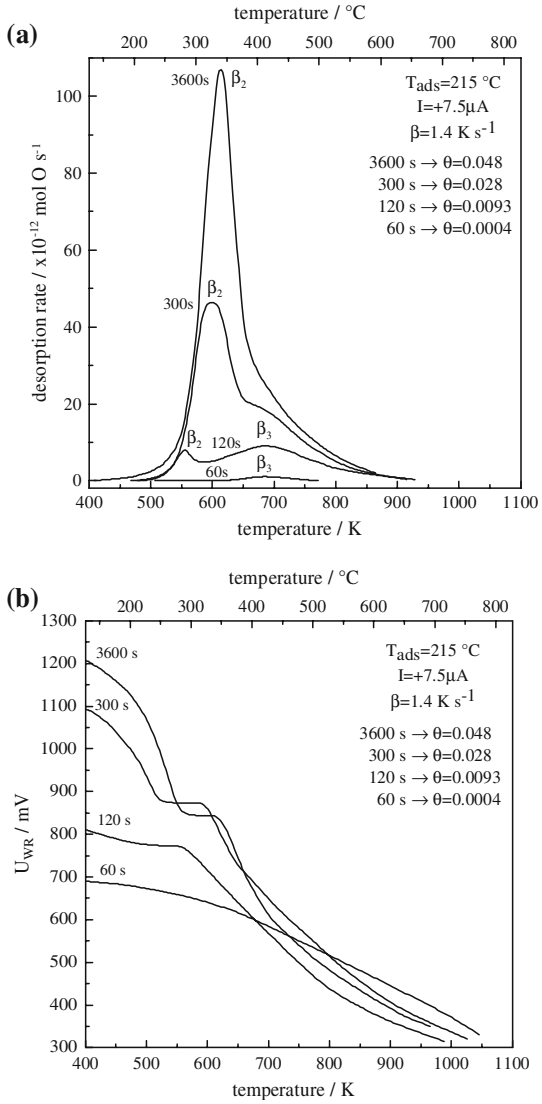

Fig. 10 (**a**) Oxygen thermal desorption spectra after electrochemical O^{2-} supply on the Pd film (I = +10 μA) through the solid electrolyte at 150 °C. The different curves correspond to various times of current application. Desorption was performed with linear heating rate, $\beta = 1.4$ °C/s. (**b**) Variation of Pd film potential versus Au reference electrode corresponding to the TPD spectra of Fig. 10a

desorption temperatures and lower applied currents. Figure 10a shows the result of electrochemical adsorption that took place at 215 °C using a constant current of 7.5 μA. In the TPD spectra we observe the formation of a second phase (state β_3) at higher desorption temperatures. This β_3 state can be well distinguished from the β_2 state at very low coverages. If we consider the reaction that transforms lattice $O^{2-}_{(YSZ)}$, which exist in the solid electrolyte, to atomic adsorbed oxygen O_{ads} ($O^{2-}_{(YSZ)} \rightarrow O^{\delta-}_{ads} \rightarrow O_{ads}$) then we can assign the state β_3 to $O^{\delta-}_{ads}$ and the state β_2 to O_{ads}. The latter (O_{ads}, state β_2) desorbs at similar temperatures than the atomic adsorbed oxygen of state β_2 does for the case of gaseous adsorption. There are still attractive interactions between the oxygen species (state β_2). These interactions are weaker than those observed at high adsorption temperatures (Fig. 9a). The open circuit potential during desorption is shown in Fig. 10b. Once again we observe the constant potential region in which we can assume that the transformation of state β_3 to state β_2 and then to $O_{2(g)}$ is taking place. Also, it is interesting to note in Fig. 10 the initial decrease of the potential, which is not accompanied by the desorption of any adsorbed species since it happens before the onset of the desorption peak. This may suggest the transformation of adsorbed species with high dipole moment into a more weakly adsorbed species (β_3 state → β_2 state).

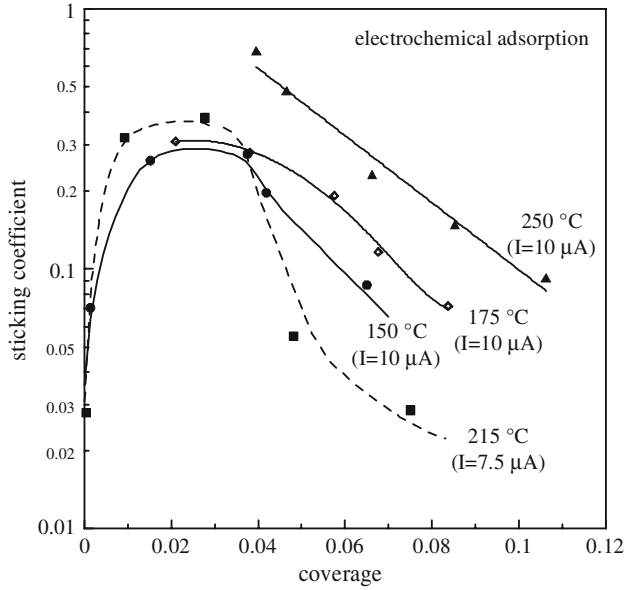

Fig. 11 Sticking coefficient as a function of coverage during electrochemical adsorption

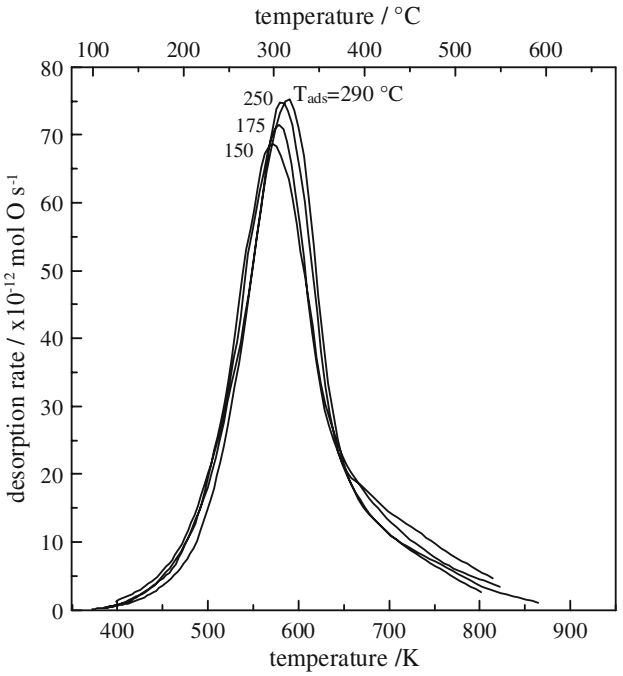

Fig. 12 Thermal desorption spectra after electrochemical O^{2-} supply through the electrolyte for 5 min. Each curve corresponds to different adsorption temperature and current in order to achieve almost the same initial coverage. Desorption was performed with linear heating rate, $\beta = 1.4$ °C/s

The sticking coefficient in electrochemical adsorption, S_e can be defined as the ratio of adsorbed oxygen molecules (calculated from integration of the TPD spectra) over the total number of oxygen atoms that are supplied through the solid electrolyte. Figure 11 shows the effect of oxygen coverage on the sticking coefficient during the electrochemical adsorption adsorption. The main points of this figure are the following:

The sticking coefficient in this case is much higher than in the gas phase adsorption, reaching a value of 0.68 for T_{ads} = 250 °C. For adsorption temperatures between 150 and 215 °C the sticking coefficient shows a peak. This behavior can be attributed to the existence of state β_3, at low coverages ($0 < \theta < 0.03$). At higher coverages (above 3%) where the state β_3 is not favored and the surface atomic oxygen dominates, the sticking coefficient starts to decrease. As a result of the high values of S, the oxygen coverages are relatively high.

In order to investigate the effect of catalyst potential on the binding strength of the atomically adsorbed oxygen, a series of low coverage thermal desorption experiments were carried out at various imposed catalyst potentials. In these experiments oxygen was supplied electrochemically and the current application value and the time of application were chosen such that the resulting initial oxygen coverage was constant for all the different applied potentials. Some of these spectra are shown in Fig. 12. Under these low coverage conditions only atomic oxygen is formed. This set of experiment was carried out at various heating rates and the modified Redhead equation of Falconer and Madix [67] was used to compute the activation energy of oxygen desorption, E_d:

$$\ln\left(\beta/T_p^2\right) = \ln\left(Rv\theta_o^{n-1}/E_d\right) - E_d/RT_p \tag{7}$$

where v is the preexponential factor, n is the desorption order, and θ_o is the initial coverage. The plot of $\ln\left(\beta/T_p^2\right)$ versus $1/T_p$ yields a straight line which is in good agreement with Eq. 7 with a slope equal to $-E_d/R$. An alternative method for the determination of E_d is the low coverage method [68, 69]. Starting again from the basic desorption rate equation (Eg. (5)) by differentiation we obtain:

$$\frac{d\ln(dN/dT)}{d(1/T)} = -\frac{E_d}{R} + \frac{d\ln(v/\beta)}{d(1/T)} + \frac{d\ln\theta}{d(1/T)} \tag{8}$$

Assuming that v and θ do not change with temperature, then we can neglect the two last terms of the above equation and obtain a slope of ln(dN/dT) versus 1/T to be equal to $-E_d/R$. This is valid only for the left "tail" of desorption spectra, that occurs at low desorption temperatures. The low coverage method is applied to the thermal desorption spectra after electrochemical O^{2-} supply at various temperatures which results to polarization of high oxygen coverage. The estimated E_d values versus catalyst potential from the two methods are potted in Fig. 13. The interesting point of this plot is that the data from both methods fall on a straight line with a slope equal to -1, with E_d to decrease between 1.31 eV and 0.90 eV as U_{WR} increases from 0.9 to 1.35 V. This

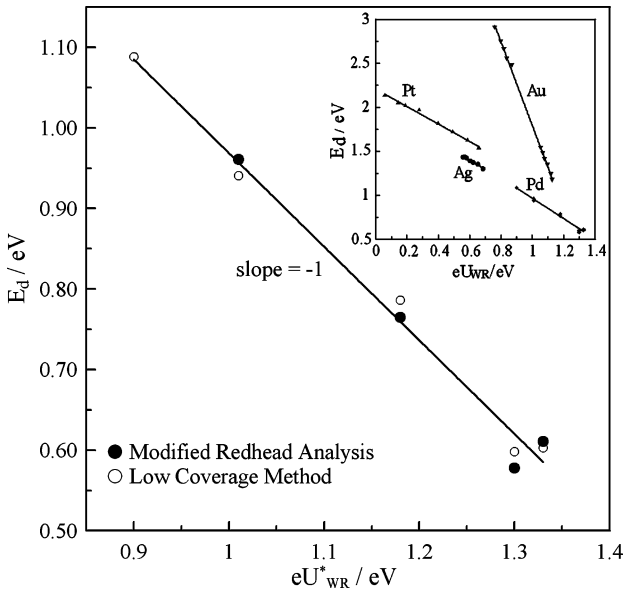

Fig. 13 Effect of catalyst potential, U^*_{WR}, on the desorption activation energy (E_d), calculated from modified Redhead analysis [67], and on the low coverage method (○) [68, 69]. Inset: Effect of catalyst potential, U^*_{WR}, on the desorption activation energies for Pt, Ag, Au and Pd [56, 57]

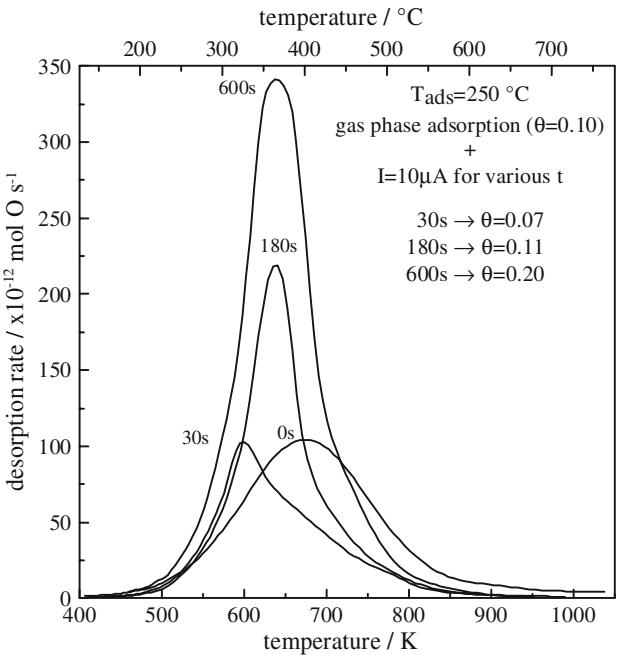

Fig. 14 Thermal desorption spectra after gaseous oxygen adsorption at 250 °C and an oxygen pressure of 3×10^{-6} Torr for 300 s (0.68 kL) followed by electrochemical O^{2-} supply for various time periods with a constant current of +10 μA. Desorption was performed with linear heating rate, $\beta = 1.4$ °C s^{-1}

confirms that the catalyst potential and work function have a pronounced effect on the binding strength of the atomic oxygen. This linear decrease of the activation energy for desorption which is related to the binding energy and to the increase of the catalyst potential and the work function is in excellent qualitative agreement with previous studies concerning Pt [56] and Ag [57]. Figure 13 (inert) shows the effect of the catalyst potential, U^*_{WR}, on the desorption activation energy for various working electrodes (Pd, Pt, Ag and Au). It has been reported for the case of Ag and observed in the present study too (for the case of Pd) that the corresponding, experimentally accessible, U^*_{WR} range is rather narrow (0.90 to 1.35 eV). This is due to the fact that any finite galvanostatically imposed positive current (e.g. O^{2-} supply to the catalyst) causes a significant increase in U^*_{WR} to values higher than 0.8 eV.

3.3 Mixed gas and electrochemical adsorption

This mode of operation has been described in the experimental section. The main results are summarized in Figs. 14 and 15. In this case, the formation of one wide peak in the oxygen TPD spectra is observed. At high desorption temperatures, the asymmetry of the spectrum indicates the existence of a second oxygen peak which is probably related to subsurface oxygen. On the other hand we observe a weaker attractive interaction between the oxygen adsorbed species compared to that observed in

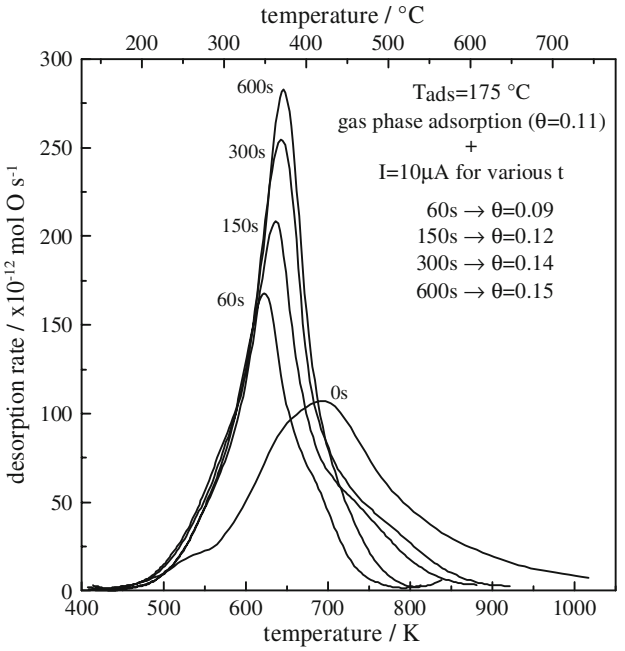

Fig. 15 Thermal desorption spectra after gaseous oxygen adsorption at 250 °C and an oxygen pressure of 3×10^{-6} Torr for 900 s (2.03 kL) followed by electrochemical O^{2-} supply for various time periods with a constant current of +10 μA. Desorption was performed with linear heating rate, $\beta = 1.4$ °C s^{-1}

purely electrochemical adsorption. The integration of the spectra leads to the conclusion that in mixed adsorption the total adsorbed oxygen is higher than in the case of the gaseous adsorption. Also, the constant potential region, which was discussed above (for purely electrochemical adsorption mode) still exists indicating the transformation between two phases (probably between β_2 and β_3). The results of the mixed adsorption are quite important since through this mode we can simulate the conditions occurring on a catalyst under electrochemical promotion conditions. In that case we have the reaction rate under open circuit conditions (which corresponds to oxygen adsorption from the gas phase) and we polarize the surface using a constant current (which corresponds in our case to oxygen supply i.e. electrochemical adsorption). By taking into consideration the results obtained under mixed adsorption we could try to correlate the TPD spectra with the experimental results of electrochemical promotion studies using Pd/YSZ catalysts.

Figure 16a, b shows the comparison of the oxygen TPD spectra obtained for the three different modes of adsorption (gaseous, electrochemical and mixed) under the same conditions at 250 °C. In Fig. 16a the oxygen exposure (for gaseous and mixed adsorption) was 0.68 kL and the amount of electrochemically supplied oxygen (for electrochemical and mixed adsorption) was 3.1×10^{-8} mol O (i.e. 10 μA for 600 s). We observe that after mixed adsorption (electrochemical promotion conditions) the amount of adsorbed oxygen is much higher than the sum of the adsorbed oxygen after electrochemical and gaseous adsorption (Fig. 16a). This is happening only for low gaseous oxygen coverages ($\theta = 0.09$, Fig. 16a). In addition, the peak desorption temperature of oxygen coming from the gas phase is higher (T_p = 410 °C) than the one observed after electrochemical and mixed adsorption (which is 370 and 360 °C respectively). Therefore electrochemical O^{2-} pumping to Pd films in the presence of preadsorbed oxygen results to the decrease of the peak desorption temperature of the atomic adsorbed oxygen from 410 to 360 °C (i.e. to a decrease of the chemisorptive binding strength of the adsorbed oxygen). Thus the atomic oxygen under positive polarization can react more easily. This is consistent with the idea, also confirmed also by XPS studies [54], that the backspillover oxide ions can act as a promoter, since they are Λ times less reactive than normally chemisorbed oxygen (see Eq. 1) [27–28]. For example if we examine the case of CH_4 oxidation, as it has been reported [29–30], there is an increase of the catalytic rate up to 9000% under positive polarization in reducing conditions

On the other hand if the catalyst surface is saturated with oxygen from the gas phase (Fig. 16b) the situation is more complex. In Fig. 16b the oxygen exposure (for gaseous and mixed adsorption) was 4.5 kL (almost saturated surface, see Fig. 2b) and the amount of electrochemically supplied oxygen (for electrochemical and mixed adsorption) was 1.55×10^{-8} mol O (i.e. 10 μA for 300 s). Due to the repulsive interactions between the adsorbed oxygen species (which were discussed in the gaseous adsorption section) the peak desorption temperature is already low (T_p = 360 °C) and the electrochemical supply of O^{2-} has almost no effect on the binding strength of O–Pd. If we

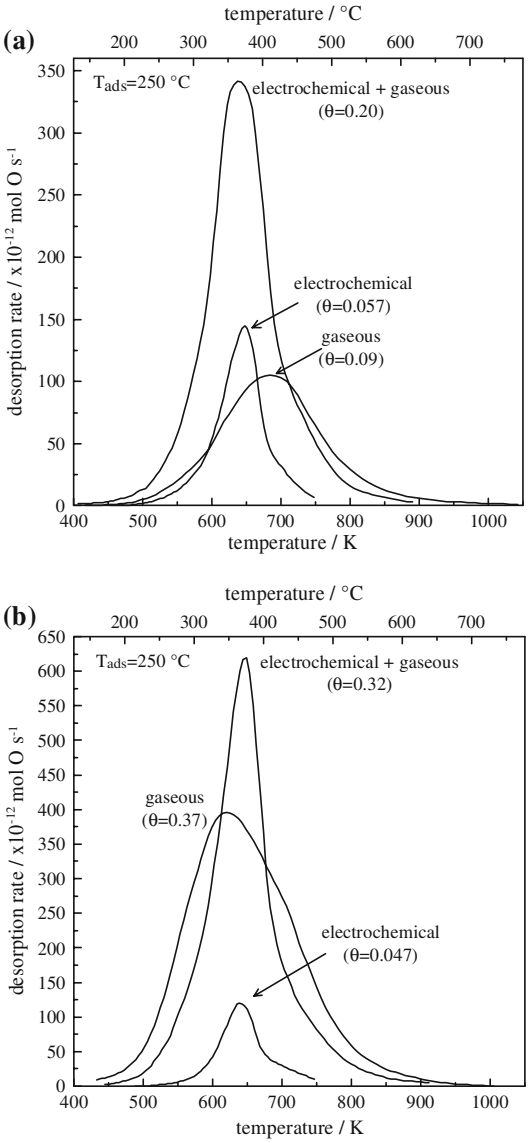

Fig. 16 Comparison of the oxygen TPD spectra obtained with the three different modes of adsorption, gaseous, electrochemical and mixed under the same conditions; (**a**) Tads = 250 °C, 0.68 kL of oxygen exposure (for gaseous and mixed adsorption) and 3.1×10^{-8} mol O of electrochemically supplied oxygen (for electrochemical and mixed adsorption), i.e. 10 μA for 600 s; (**b**) Tads = 250 °C, 4.5 kL of oxygen exposure (for gaseous and mixed adsorption) and 1.55×10^{-8} mol O of electrochemically supplied oxygen (for electrochemical and mixed adsorption), i.e. 10 μA for 300 s

examine the example of C_2H_4 oxidation under positive polarization and oxidizing conditions [48] the effect of the potential in the catalytic rate is very small ($\rho = 1.45$). Considering that O_2 is adsorbed on Pd more strongly than C_2H_4 [3, 74] and that no effect of electrochemically O^{2-} supply on binding strength of the atomic oxygen is expected under saturated oxygen conditions, then the above result (small value of ρ) concerning the C_2H_4 oxidation over Pd in oxidizing conditions becomes easy to rationalize.

4 Conclusions

The main conclusions are:

1. Gaseous oxygen adsorption gives two adsorbed atomic oxygen species desorbing at about 300 °C (state β_1) and 340–500 °C (state β_2). The creation of the low temperature state is favored at high exposure times (exposure >1 kL) and low adsorption temperatures ($T_{ads} < 200$ °C) and is associated with the decrease of the oxygen dipole moment at high coverages. Electrochemical O^{2-} pumping to the Pd catalyst causes the creation of two peaks (at 350 and 430 °C) corresponding to O_{ads} and $O_{ads}^{\delta-}$ according to the following reaction:

   $$O^{2-}_{(YSZ)} \rightarrow O^{\delta-}_{ads} \rightarrow O_{ads}$$

   The formation of the$O_{ads}^{\delta-}$ oxygen is an intermediate stage before the formation of the atomic adsorbed oxygen, O_{ads}. The weakly bonded state, O_{ads} desorbs at temperatures similar to the ones of the oxygen of the state β_1, after gaseous adsorption. In the case of a non-saturated with oxygen surface, supply of O^{2-} ions results to a decrease in the chemisorptive binding strength of atomic oxygen, making it more reactive.

2. The total amount of adsorbed oxygen is much higher in the case of mixed adsorption than in the case of gaseous or electrochemical adsorption
3. Desorption activation energy of oxygen decreases linearly with increasing catalyst potential. This decrease implies a pronounced increase in the desorption rate of the adsorbed oxygen at any fixed temperature and thus to an increase in the reactivity of adsorbed oxygen for catalytic oxidation reactions.

Acknowledgements The author would like to thank Professor Costas Vayenas from University of Patras for helpful discussions and his support, friendship and trust during the last 10 years. I am also very thankful to Professor George Karatzas and especially to my reviewers for their very thorough review and numerous very helpful suggestions.

References

1. Ertl G, Rau P (1969) Surf Sci 15:443
2. Ertl G, Kueppers J (1970) Surf Sci 21:61
3. Conrad H, Ertl G, Kueppers J, Latta EE (1977) Surf Sci 65:245
4. Conrad H, Ertl G, Kueppers J (1978) Surf Sci 76:323
5. Matsushima T (1985) Surf Sci 157:85
6. Guo X, Hoffman A, Yates JT (1989) J Phys Chem 90:5787
7. Weissman DL, Shek ML, Spicer WE (1980) Surf Sci 92:L59
8. Imbihl R, Demuth JE (1986) Surf Sci 173:395
9. Zheng G, Altman EI (2000) Surf Sci 462:151
10. Voogt EH, Mens AJM, Gijzeman OLJ, Geus JW (1997) Surf Sci 373:219
11. Stuve EM, Madix RJ, Brundle CR (1984) Surf Sci 146:155
12. Chang SL, Thiel PA (1988) J Phys Chem 88:2071
13. Klier K, Wang YN, Simmons GW (1993) Surf Sci 97:633
14. He JW, Norton PR (1988) Surf Sci 204:26
15. He JW, Memmert U, Norton PR (1989) J Phys Chem 90:5088
16. Bondzie VA, Kleban P, Dwyer DJ (1986) Surf Sci 347:395
17. Milun M, Pervan P, Vajic M (1989) Surf Sci 211/212:887
18. Yagi K, Sekiba D, Fukutani H (1999) Surf Sci 442:307
19. Campbell CT, Foyt DC, White JM (1977) J Phys Chem 81:491
20. Putna ES, Vohs JM, Gorte RJ (1997) Surf Sci 391:L1178
21. Xu X, Goodman DW (1993) J Phys Chem 97:7711
22. Lintz HG, Vayenas CG (1989) Angewandte Chemie Intern Ed in Engl 28:708
23. Vayenas CG, Bebelis S, Neophytides S, Yentekakis IV (1989) Appl Phys A 49:95
24. Nicole J, Tsiplakides D, Pliangos G, Verykios XE, Comninellis C, Vayenas CG (2001) J Catal 204:23
25. Vayenas CG, Bebelis S, Neophytides S (1988) J Phys Chem 92:5083
26. Vayenas CG, Bebelis S, Ladas S (1990) Nature 343:625
27. Vayenas CG, Bebelis S, Pliangos C, Brosda S, Tsiplakides D (2001) Electrochemical activation of catalysis: promotion, electrochemical promotion and metal-support interactions. Kluwer Academic/Plenum Publishers, New York
28. Vayenas CG, Jaksic MM, Bebelis S, Neophytides SG (1996) In: Bockris JOM, Conway BE, White RE (eds) Modern aspects of electrochemistry, vol. 29. Kluwer Academic/Plenum Publishers, New York
29. Frantzis AD, Bebelis S, Vayenas CG (2000) Solid State Ionics 136–137:863
30. Giannikos A, Frantzis AD, Pliangos C, Bebelis S, Vayenas CG (1998) Ionics 4:53
31. Politova TI, Sobyanin VA, Belyaev VD (1990) React Kinet Catal Lett 41:321
32. Basini L, Cavalca CA, Haller GL (1994) J Phys Chem 98:10853
33. Harkness I, Lambert RM (1995) J Catal 152:211
34. Chiang PH, Eng D, Stoukides M (1993) J Catal 139:683
35. Constantinou I, Bolzonella I, Pliangos C, Comninellis C, Vayenas CG (2005) Catal Lett 100:125
36. Cavalca CA, Haller GL (1998) J Catal 177:389
37. Palermo A, Tikhov MS, Filkin NC, Lambert RM, Yentekakis IV, Vayenas CG (1996) Stud Surf Sci Catal 101:513
38. Cavalca C, Larsen G, Vayenas CG, Haller G (1993) J Phys Chem 97:6115
39. Vayenas CG, Michaels J (1982) Surf Sci 120:L405
40. Vayenas CG, Debeneddi PG, Yentekakis Y, Hegedus LL (1985) Ind & Eng Chem Fund 24:316
41. Pliangos C, Yentekakis IV, Ladas S, Vayenas CG (1996) J Catal 159:189
42. Neophytides S, Tsiplakides D, Stonehart P, Jaksic M, Vayenas CG (1994) Nature 370:292

43. Balomenou S, Tsiplakides D, Katsaounis A, Thiemann-Handler S, Cramer B, Foti G, Comninellis C, Vayenas CG (2004) Appl Catal B: Environ 52:181
44. Balomenou SP, Tsiplakides D, Katsaounis A, Brosda S, Hammad A, Foti G, Comninellis C, Thiemann-Handler S, Cramer B, Vayenas CG (2006) Solid State Ionics 177:2201
45. Grzybowska-Swierkosz B, Haber J (1994) Annual reports on the progress of chemistry. The Royal Society of Chemistry, Cambridge
46. Pritchard J (1990) Nature 343:592
47. Bockris JOM , Minevski ZS (1974) Electrochim Acta 39:1471
48. Yiokari K, Bebelis S (2000) J Appl Electrochem 30:1277
49. Marwood M, Vayenas CG (1997) J Catal 170:275
50. Luerssen B, Gónther S, Marbach H, Kiskinova M, Janek J, Imbihl R (2000) Chem Phys Lett 316:331
51. Makri M, Vayenas CG, Bebelis S, Besocke KH, Cavalca C (1996) Surf Sci 369:351
52. Vayenas CG, Archonta D, Tsiplakides D (2003) J Electroanal Chem 554–555:301
53. Archonta D, Frantzis A, Tsiplakides D, Vayenas CG (2006) Solid State Ionics 177:2221
54. Ladas S, Kennou S, Bebelis S, Vayenas CG (1993) J Phys Chem 97:8845
55. Kondarides DI, Papatheodorou GN, Vayenas VG, Verykios XE (1993) Berichte Bunsengesellschaft der Physikalischen Chemie 97:709
56. Neophytides S, Tsiplakides D, Vayenas CG (1998) J Catal 178:414
57. Tsiplakides D, Vayenas CG (1999) J Catal 185:237
58. Stoukides M, Vayenas CG (1984) J Electrochem Soc 131:839
59. Neophytides SG, Vayenas CG (1995) J Phys Chem 99:17063
60. Katsaounis A, Nikopoulou Z, Verykios XE, Vayenas CG (2004) J Catal 222:192
61. Katsaounis A, Nikopoulou Z, Verykios XE, Vayenas CG (2004) J Catal 226:197
62. Zipprich W, Wiemhφfer H-D, Vöhrer U, Göpel W (1995) Berichte Bunsengesellschaft der Physikalischen Chemie 99:1406
63. Ladas S, Bebelis S, Vayenas CG (1991) Surf Sci 251/252:1062
64. Nicole J, Tsiplakides D, Wodiunig S, Comninellis C (1997) J Electrochem Soc 144:L312
65. Anderson JR (1975) Structure of metallic catalysts. Academic Press, London
66. Bebelis S, Vayenas CG (1992) J Catal 138:570
67. Falconer JL, Madix RJ (1975) Surf Sci 48:393
68. Ibach H, Erley W, Wagner H (1980) Surf Sci 92:29
69. Habenshaden E, Kueppers J (1984) Surf Sci 138:L147
70. Hoffman A, Guo X, Yates JT, Gadzuk JW, Clark CW (1989) J Phys Chem 90:5793
71. Goschnick J, Wolf M, Grunze M, Unertl WN, Block JH, Loboda-Cackovic J (1986) Surf Sci 178:831
72. Leisenberger FP, Koller G, Sock M, Surnev S, Ramsey MG, Netzer FP, Kloetzer B, Hayek K (2000) Surf Sci 445:380
73. Kloetzer B, Hayek K, Konvicka C, Lundgren E, Varga P (2001) Surf Sci 482–485:237
74. Tysoe WT, Nyberg GL, Lambert RM (1984) J Phys Chem 88:1960